Objective Model Selection for Identifying the Human Feedforward Response in Manual Control

Drop, Frank; Pool, Daan; van Paassen, Rene; Mulder, Max; Bülthoff, Heinrich H.

DOI
10.1109/TCYB.2016.2602322

Publication date
2017

Document Version
Accepted author manuscript

Published in
IEEE Transactions on Cybernetics

Objective Model Selection for Identifying the Human Feedforward Response in Manual Control

Frank M. Drop, *Student member, IEEE,* Daan M. Pool, *Member, IEEE,* Marinus (René) M. van Paassen, *Senior member, IEEE,* Max Mulder, Heinrich H. Bülthoff, *Member, IEEE*

***Abstract*—Realistic manual control tasks typically involve predictable target signals and random disturbances. The human controller (HC) is hypothesized to use a feedforward control strategy for target-following, in addition to feedback control for disturbance-rejection. Little is known about human feedforward control, partly because common system identification methods have difficulty in identifying whether, and (if so) how, the HC applies a feedforward strategy. In this paper an identification procedure is presented that aims at an objective model selection for identifying the human feedforward response, using linear time-invariant ARX models. A new model selection criterion is proposed to decide on the model order (number of parameters) and the presence of feedforward in addition to feedback. For a range of typical control tasks, it is shown by means of Monte Carlo computer simulations that the classical Bayesian Information Criterion (BIC) leads to selecting models that contain a feedforward path from data generated by a pure feedback model: 'false-positive' feedforward detection. To eliminate these false-positives, the modified BIC includes an additional penalty on model complexity. The appropriate weighting is found through computer simulations with a hypothesized HC model *prior* to performing a tracking experiment. Experimental human-in-the-loop data will be considered in future work. With appropriate weighting, the method correctly identifies the HC dynamics in a wide range of control tasks, without false-positive results.**

***Index Terms*—Manual control, feedforward control, human control models, system identification, parameter estimation**

I. Introduction

MANUAL control of a dynamic system typically requires the human controller (HC) to steer that system, perturbed by disturbances, along a reference trajectory. An example is the manual control of an aircraft during turns and landings, in the presence of turbulence. The HC will use all available information and knowledge, i.e., visual, vestibular, and somatosensory information as well as prior experience, to improve control performance and reduce effort [1]–[5].

In many everyday control situations the reference trajectory or target signal has a simple and predictable waveform. Evidence exists that in this case the HC employs a feedforward control strategy, as it can considerably improve tracking performance, without affecting closed-loop stability [6]–[8]. Feedforward control plays an essential role in many neurophysiological processes as well [9]–[12].

Although feedforward control strategies were frequently hypothesized [1], [6]–[8], [13], [14] and some empirical evidence was provided [15], [16], it was only until recently that feedforward control was studied by means of system identification and parameter estimation techniques [17]–[19] with the goal of modeling the feedforward in detail.

System identification techniques allow us to experimentally measure *if*, and mathematically model *how* the HC responds to multiple sources of information. Many of the common techniques [1], [13], [20]–[26], however, were not designed to identify the feedforward response in addition to the, relatively well-known, feedback response.

The main problem is that, given a particular manual control task, it is often not known a priori whether the HC will exert feedforward control, or not. Adding a feedforward path to the HC model adds degrees of freedom in the model (more parameters) that the identification method can use to obtain a better fit. When the model selection is only based on the 'best' quality of fit, the identification procedure is likely to be biased towards selecting more complex models. The choice for including a feedforward path might be a 'false-positive' result. A secondary problem is that it is often unknown *how* the human feedforward and feedback paths should be modeled. Although basic control-theoretical insights provide a good initial guess, prior assumptions on the feedforward dynamics cannot be based on previous experimental results, because hardly any literature exists on the subject.

It is the goal of this paper to address and resolve these two issues, and describe an objective identification procedure to simultaneously identify the HC feedforward and feedback control responses. To address the first issue, the procedure selects the best model based on a trade-off between model complexity (the model order) and the model quality-of-fit. To address the second issue, it uses *un*constrained linear models which allows the selection of the best global model available.

In short, the proposed identification procedure will identify many different linear time invariant (LTI) autoregressive with exogenous input (ARX) models [27]. The models vary in the model structure (pure feedback and combined feedback-feedforward response models are considered), and in the number of model parameters (model order). A model selection criterion, derived from the Bayesian Information Criterion (BIC) [27], [28] is used to choose the best model. It decides on the model order and whether a feedforward component is needed, or not, to describe the data. This differs from previous ARX estimation procedures, where no explicit model order selection step was used [21]–[23], [25]

The functionality of the proposed procedure is assessed by means of computer simulations, because it is necessary to know the true model to assess the ability of the procedure

F. M. Drop and H. H. Bülthoff are with the Max Planck Institute for Biological Cybernetics, Tübingen (Germany), {frank.drop, hhb}@tuebingen.mpg.de. All other authors are with the Control and Simulation section, Faculty of Aerospace engineering, Delft University of Technology (Netherlands).

to identify the true dynamics. It is found that the original BIC does not weigh the model complexity enough, such that 'false-positive' feedforward identification occurs frequently. This problem is addressed by altering the relative weighting of model quality and model complexity in the model selection criterion, by the introduction of a 'model complexity penalty parameter' in the selection criterion as suggested by Ljung [27]. The weighting is tuned by means of offline Monte Carlo simulations with a HC model based on literature. The procedure is applied to experimental data in future work.

The paper is structured as follows. Section II provides an overview of the identification problem, our workflow and proposed procedure. Sections III and IV describe in more detail the individual steps in the procedure. Sections V to VII discuss the results of applying the procedure to a comprehensive example, involving four typical manual control tasks. The paper concludes with a discussion and conclusions.

II. Identification Problem and Approach

Section II introduces the general identification problem and provides an overview of the steps in the procedure. Section III and IV describe ARX model identification and our tuning of the model selection criterion, respectively, in detail.

A. Identification problem and objectives

This paper focuses on the identification of human control behavior in a combined target-tracking and disturbance-rejection task, with predictable target signals and unpredictable disturbances. Here, the task resembles an aircraft pitch attitude control task. Fig. 1 illustrates the task: the HC controls a dynamic system Y_c such that the output θ (perturbed by disturbance f_d) accurately follows the target f_t. Thus, the error e, defined as $e = f_t - \theta$, is minimized. The target f_t and disturbance f_d signals are referred to as *forcing functions*.

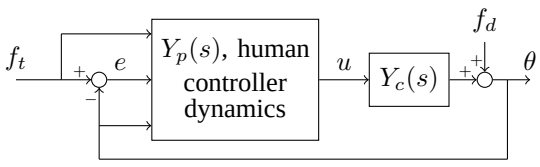

Fig. 1. Control scheme studied here. The HC perceives the target signal f_t, the perturbed system output θ and the error e from a pursuit display and generates control signal u.

System identification and parameter estimation methods are used to address four objectives: O.1) to identify the signals to which the HC responds in a particular task; these are the input signals of the HC model; O.2) to identify the governing HC dynamics, in the frequency range where they contribute most to the model output signal u; O.3) to obtain a precise and physically meaningful parametrization of the HC model; and O.4) to quantify changes in those dynamics as a function of control task variables. A single method suitable for all four objectives does not exist. These four objectives should be addressed sequentially by specific methods and the results of one step are necessary for the next. However, previous studies into manual feedforward addressed O.4 directly, relying on models derived from control theoretical insights rather than system identification results [17], [18].

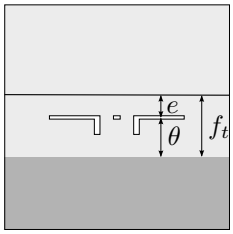

Fig. 2. Pursuit display for aircraft pitch control. The horizontal black line indicates the target pitch attitude f_t, the aircraft symbol indicates the current pitch attitude θ, and thus the vertical distance between the target and the aircraft symbol is the error e. The display only shows the current values of the signals; no past/preview information is available.

The objective of the procedure described here is to simultaneously address O.1 and O.2, providing the insights necessary to parametrize the model (O.3). The procedure does *not* aim to address O.4; existing parameter estimation methods work satisfactory and are currently not limiting manual control research [26]. Objectives O.1 and O.2 involve five challenges.

First, the HC is presented with three signals on a pursuit display, Fig. 2: f_t, e and θ, and can respond to all three (but possibly also to two, or even just one). Because of the linear relationship $e = f_t - \theta$, however, only the responses to two input signals can be identified [7]. The two responses to be identified can be chosen freely; all choices are equivalent from an identification point of view. For this particular control task, we choose to identify the feedforward response on the target f_t and the feedback response on the error e. A feedforward and feedback model likely reflects the actual control strategy best, as we consider *predictable* target signals [17]. Other control tasks may require a different choice of possible HC responses.

Second, the HC is a highly adaptive, nonlinear controller and will change the control strategy to the characteristics of Y_c and the properties of the forcing functions f_t and f_d. Therefore, the HC response needs to be measured in a control task very similar to the task for which the identified model will be used, and the identification procedure should be compatible with the chosen forcing functions and system dynamics. Realistic control tasks often involve ramp or parabola-like reference signals, which have power at all frequencies. This renders non-parametric techniques that rely on the excitation of the HC at discrete frequencies useless [13], [24]. Hence, the procedure introduced here is based on multi-input, single-output (MISO) linear time-invariant (LTI) ARX models [27] that pose less stringent requirements on forcing function properties.

Third, a relatively large portion of the HC control signal is not (linearly) correlated to any of the input signals presented to the HC, and thus cannot be described by a linear model. This modeling residual, designated n, is *human remnant* and consists of the unmodeled nonlinear dynamics and random noise. The remnant level (expressed as the variance of the remnant over the variance of the control signal, σ_n^2/σ_u^2) is usually large, up to 30% [26], and is a key complicating factor in the identification of small, yet relevant control dynamics. To

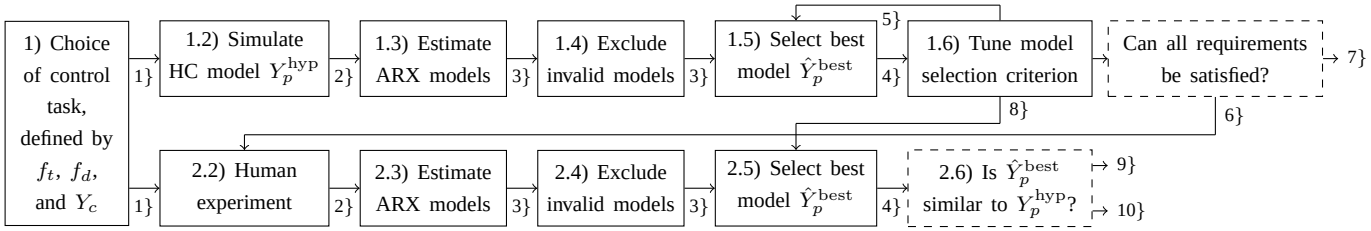

Fig. 3. Workflow of the procedure proposed in this paper. Circled numbers denote outputs of the steps. 1} f_t, f_d, Y_c, and remnant power σ_n^2/σ_u^2. 2} e_m, u_m. 3} Set of $\hat{Y}_p$ with corresponding $\hat{u}_m$. 4} $\hat{Y}_p^{\mathrm{best}}$, $\hat{u}_m^{\mathrm{best}}$. 5} Increase/decrease model complexity weighting. 6} **Yes:** phase 2, human-in-the-loop experiment, can commence. 7} **No:** make changes to control task or experimental paradigm, go back to 1). 8} Tuned model selection criterion weighting. 9} **Yes:** phase 1 was performed for the correct Y_p^{hyp}. 10} **No:** adjust Y_p^{hyp} and go back to 1.2.

reduce the remnant level, experimental data is averaged over multiple recordings before it is further analyzed.

Fourth, the use of MISO LTI ARX models for identification purposes requires the user to choose the appropriate number of model parameters (the model order), and the time delay for *each* of the model inputs. In the proposed identification procedure we will use a model selection criterion derived from the Bayesian Information Criterion (BIC) [28] to objectively determine the model order and time delay values. The model selection criterion must prevent *overfitting*, the selection of a model with too many (meaningless) parameters. It takes into account both the model *quality*, the goodness of the model fit, and the model *complexity*, the model order, in the choice for the 'best' model. Although the primary objective of the model selection criterion is to prevent overfitting, by putting a certain weight on model complexity, it is equally important to prevent *underfitting* by putting too much weight on model complexity. Our procedure will explicitly address this weighting.

Fifth, all measurements need to be taken in *closed-loop*. This causes the tracking error e (one of the model inputs) to be correlated with the noise (human remnant) present in the control signal u (the model output). That is, apart from the 'forward' relationship between e and u (that is to be identified), an additional correlation exists, equal to $-1/Y_c$, due to the closed-loop feedback [29, pp. 19], [30]. At frequencies where remnant is larger than the disturbance signal this correlation $-1/Y_c$ might be identified [20]. 'Indirect' identification methods are less sensitive [30] to these closed-loop effects than the classic 'direct' [27] identification approach. Indirect identification methods, however, often consist of more steps yielding a more involved procedure or tend to return models of unnecessarily high order [30], which is unacceptable for our objective. Thus, we apply a direct identification approach.

B. Approach

The identification procedure introduced in this paper reflects the workflow we recommend when performing studies on HC behavior. It is illustrated in Fig. 3.

The workflow consists of two phases. In the first phase, the procedure is applied to data obtained by *simulating* an HC model that is hypothesized for the control task at hand, with numerous remnant realizations. Using this simulation data set, a Monte Carlo analysis is performed to assess whether the procedure is indeed able to identify the HC model and, most importantly, to *tune* the model selection criterion. When successful in identification of the simulated HC model and the criterion being tuned to satisfaction, the second phase commences and the procedure is applied to the experimental data using the obtained model selection criterion tuning. The individual steps are briefly introduced below.

1) The control task is defined by the chosen target signal f_t, disturbance signal f_d, and system dynamics Y_c. For this control task, based on existing literature or control-theoretic principles, a model for the HC, Y_p^{hyp}, is hypothesized. Here, Y_p^{hyp} is a MISO system with inputs f_t and e, and output u. The experimental paradigm will determine the remnant level σ_n^2/σ_u^2 for which the procedure has to be evaluated.

1.2) Many (100+) different remnant realizations are generated, such that the simulation data set has a sufficient level of randomness to reflect the nonlinear human response.

1.3) Many different MISO ARX models are estimated from the collected data. The signals used to estimate the ARX models are the two model inputs: the target signal f_t and the measured tracking error e_m; and the model output signal: the measured control signal u_m. Each estimated ARX model $\hat{Y}_p$ is simulated to obtain the estimated control signal $\hat{u}_m$.

1.4) The validity of the ARX models from an identification point-of-view is tested and invalid models are excluded. Models with dynamics (poles and zeros) outside the frequency range excited by the forcing functions are considered invalid.

1.5) The best ARX model $\hat{Y}_p^{\mathrm{best}}$, with corresponding $\hat{u}_m^{\mathrm{best}}$, is selected through a model selection criterion that trades off model complexity and model quality. For simulated data, this trade-off is tuned until all requirements at step 1.6 are satisfied.

1.6) Simultaneously, the model selection criterion is tuned *and* the ability of the procedure to correctly identify Y_p^{hyp} is assessed by means of four quantitative requirements, that are chosen by the user depending on the objectives of the study: R.1) 'False-positive' identification of one or more responses should occur in fewer than η_{fp} realizations, where η_{fp} is a percentage chosen by the user. R.2) The selected model is the *best of all evaluated models*, but not necessarily a good model in an absolute sense. Therefore, $\hat{u}_m^{\mathrm{best}}$ is compared to u_m to assess the time-domain quality-of-fit. The quality-of-fit should surpass a level chosen by the user. R.3) The selected model $\hat{Y}_p^{\mathrm{best}}$ should be sufficiently complex to describe dynamics of the same order as Y_p^{hyp}. R.4) The response dynamics of Y_p^{best} should be sufficiently similar to Y_p^{hyp}.

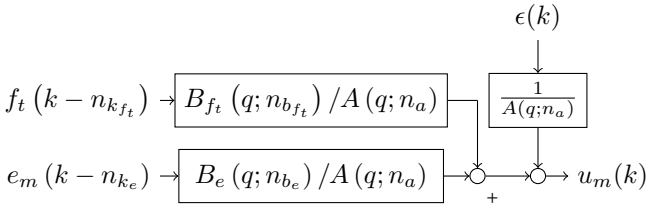

Fig. 4. Generic ARX model structure.

The main result of step 1.6, i.e., with the simulated data, is that the model selection criterion is tuned to the HC behavior expected for the control task being studied, such that the procedure reliably selects a model similar to Y_p^{hyp}. If all requirements cannot be satisfied simultaneously, the control task or experimental paradigm needs to be changed to excite the relevant HC dynamics more, or reduce the remnant levels.

The requirements imposed by 1.6 are assessed as a function of the relative weighting of model complexity and model quality at step 1.5. For simulated data, the 'true' dynamics Y_p^{hyp} are perfectly known and thus it is possible to *tune* the model selection criterion such that $\hat{Y}_p^{\text{best}}$ is most similar to Y_p^{hyp}. Most importantly, repeating the procedure for all individual remnant realizations allows us to assess the occurrences of 'false-positive' and 'false-negative' results, and see how the relative weighting needs to be tuned to minimize these objective, yet *invalid*, model selections.

The steps of phase 2 are identical to the corresponding steps in phase 1, with the following exceptions.

2.2) Experimental human-in-the-loop data are collected from a number of participants.

2.5) The model selection criterion uses the tuning obtained in step 1.6, i.e., the model selection is not tuned in phase 2.

2.6) The model $\hat{Y}_p^{\text{best}}$ that was identified from *experimental* data is compared to Y_p^{hyp}, to assess whether the Monte Carlo analysis was performed for the correct model. In case discrepancies between $\hat{Y}_p^{\text{best}}$ and Y_p^{hyp} are substantial, phase 1 should be repeated using a model more similar to the experimentally found $\hat{Y}_p^{\text{best}}$. If $\hat{Y}_p^{\text{best}}$ identified from experimental data is indeed very similar to Y_p^{hyp} (confirming the HC model hypothesis), Y_p^{hyp} can be used for O.3 and O.4.

III. ARX Identification and Model Selection

The ARX model estimation, evaluation and selection steps (1.3 through 1.5 in Fig. 3) are an essential part of the identification procedure. They are described in detail next.

Step 1.3, substep A. The data are time traces of f_t, e_m, and u_m, lasting 81.92 s and sampled at 100 Hz. These are split into an estimation set ($t = [0, 40.95]$ s) and a validation set ($t = [40.96, 81.91]$ s). Data are resampled to 25 Hz after filtering to prevent aliasing, yielding 1024 samples data sets. Resampling reduces computation effort, but may introduce biases in the estimated models. The estimated time delays are affected most, as these can only be integer multiples of the sample time.

Step 1.3, substep B. Many ARX models are fit onto the estimation data. The generic structure of each ARX model is shown in Fig. 4 and is described by the discrete-time difference equation (1), with k the discrete time samples of 0.04 s:

$$\begin{aligned} A(q;n_a)u_m(k) = \quad & B_{f_t}(q;n_{b_{f_t}})f_t(k-n_{k_{f_t}})+ \\ & B_e(q;n_{b_e})e_m(k-n_{k_e})+\epsilon(k) \end{aligned} \tag{1}$$

Here, ϵ is a white noise signal, q is the delay operator and the polynomials A, B_{f_t}, and B_e are defined as:

$$\begin{aligned} A(q;n_a) &= 1+a_1q^{-1}+\ldots+a_{n_a}q^{-n_a} \\ B_{f_t}(q;n_{b_{f_t}}) &= b_{f_t,1}+b_{f_t,2}q^{-1}+\ldots+b_{f_t,n_{b_{f_t}}}q^{\left(-n_{b_{f_t}}+1\right)} \\ B_e(q;n_{b_e}) &= b_{e,1}+b_{e,2}q^{-1}+\ldots+b_{e,n_{b_e}}q^{(-n_{b_e}+1)} \end{aligned} \tag{2}$$

Each ARX model is described by three model orders, i.e., the number of parameters in the A polynomial (n_a), the B_{f_t} polynomial ($n_{b_{f_t}}$), and the B_e polynomial (n_{b_e}). For each of the two input signals, a delay parameter needs to be identified: the feedforward time delay $n_{k_{f_t}}$, and the feedback time delay n_{k_e}, both integer multiples of the sample time 0.04 s.

The *effective* total number of free parameters d of each ARX model is the sum of n_a, $n_{b_{f_t}}$, and n_{b_e}, plus the total number of delays in the model. That is, for a pure feedback model with $n_{b_{f_t}} = 0$ and $n_{b_e} > 0$, the number of free parameters d equals $n_a + n_{b_e} + 1$. For a pure feedforward model, with $n_{b_{f_t}} > 0$ and $n_{b_e} = 0$, $d = n_a + n_{b_{f_t}} + 1$. For a combined feedback-feedforward model, with $n_{b_{f_t}} > 0$ and $n_{b_e} > 0$, $d = n_a + n_{b_{f_t}} + n_{b_e} + 2$.

Each model order and delay parameter is varied over a certain range, and the full factorial combination of these ranges results in a huge number of model candidates. The ranges depend on the expected complexity and time delay of the HC responses, where a more complex response requires more parameters. The identification procedure is more objective if the evaluated range is large, at the cost of computation time.

Step 1.3, substep C. Each model is evaluated by *simulating* the f_t and e_m signals through the estimated model to obtain $\hat{u}_m$, the estimate of the measured control signal u_m. The full 81.92 s of data are used to simulate the model and obtain $\hat{u}_m$, but only the last 40.96 s (the validation data set) are used to calculate the quality of the fit V, with N_d = 1024:

$$V = \frac{1}{N_d}\sum_{k=N_d+1}^{2N_d}\left(\hat{u}_m(k)-u_m(k)\right)^2, \tag{3}$$

Step 1.4. The validity of each ARX model from an identification perspective is assessed and 'invalid' models are excluded. The HC dynamics can be identified only within the frequency range where both forcing functions f_t and f_d have power. Outside this frequency range only noise is measured.

Early evaluations of the identification procedure revealed that ARX models containing dynamics approximating $-1/Y_c(s)$ were selected in a small number of cases, see Section II-A. These models provided a good fit, because in addition to fitting the HC control dynamics (that are to be identified), they could also fit the correlation between e and the remnant at higher frequencies caused by taking measurements in closed-loop. The use of separate estimation and validation data sets does not prevent the selection of these models,

because this relation is 'real'. These models are excluded by checking for the presence of zeros in the feedback path of the ARX model close to, or above the highest frequency component in the disturbance signal f_d.

Step 1.5. The model selection criterion is calculated for each model from the quality of fit V and model complexity expressed by the number of parameters d. The model with the smallest value is selected as the best model. The selection criterion used is a modified version of the Bayesian Information Criterion (BIC), defined as [27]:

$$\mathrm{BIC} = \log V + \frac{d \log N_d}{N_d}. \tag{4}$$

The trade-off between model quality and complexity by the BIC is fixed. Yet, each control task has its own particularities and for some studies the original BIC might either put too much weight on model complexity, such that certain HC dynamics are overseen, underfitting, or too little weight, leading to overfitting. Therefore, in our identification procedure an additional parameter c is introduced to allow the trade-off to be *tuned* [27], yielding the modified BIC (mBIC):

$$\mathrm{mBIC} = \log V + c\frac{d \log N_d}{N_d} \tag{5}$$

The 'model complexity penalty parameter' c is to be tuned by means of computer simulations, such that false-positives are avoided, while maintaining sensitivity to small yet important contributions of certain HC control dynamics. For a given value of c, the model with the lowest mBIC value is selected to be the best model $\hat{Y}_p^{\mathrm{best}}$.

IV. Model Selection Criterion Tuning

The main innovation in the identification procedure lies in the tuning of the model selection parameter c at step 1.6 guided by four tangible requirements described in detail next. Note that this tuning process happens with the simulated data only.

R.1) 'False-positive' identification of a response should occur in fewer than η_{fp} realizations. The order of the path in $\hat{Y}_p^{\mathrm{best}}$ associated to a response that is not present in Y_p^{hyp} should be equal to zero. E.g., $n_{b_{f_t}}$ should be zero for data generated by a pure feedback model. If false-positives are found in more than η_{fp} realizations, c should be increased.

R.2) The time-domain quality of fit of the selected ARX model $\hat{Y}_p^{\mathrm{best}}$ is evaluated, by comparing its control signal $\hat{u}_m^{\mathrm{best}}$ to the measured control signal u_m in the time domain. Previous literature measured the fit quality using the Variance Accounted For (VAF) [17], [18], defined as:

$$\mathrm{VAF} = \left(1 - \frac{\sum_{k=N_d+1}^{2N_d} \left(u_m(k) - \hat{u}_m(k)\right)^2}{\sum_{k=N_d+1}^{2N_d} \hat{u}_m(k)^2}\right) \times 100\%. \tag{6}$$

The VAF of $\hat{Y}_p^{\mathrm{best}}$ is to be compared to the VAF of Y_p^{hyp}, by means of the *VAF ratio* defined as VAF($\hat{Y}_p^{\mathrm{best}}$) / VAF($Y_p^{\mathrm{hyp}}$). A VAF ratio larger than 1 is an indication of overfitting; $\hat{Y}_p^{\mathrm{best}}$ was able to fit the remnant and c should be made larger to prevent this. A VAF ratio smaller than 1 indicates underfitting. The user chooses an allowable range for the VAF ratio depending on the importance of preventing overfitting over obtaining a model providing a high model quality.

R.3) Feedforward ARX models ($n_{b_{f_t}} > 0$) should be identified from data generated by a combined feedback-feedforward HC model (with $K_{p_t} > 0$). Moreover, the selected ARX model $\hat{Y}_p^{\mathrm{best}}$ should be sufficiently complex to describe the dynamics of Y_p^{hyp}. For example, if the feedforward in Y_p^{hyp} is a differentiator, then $n_{b_{f_t}}$ should be equal to or larger than 2 to describe these dynamics accurately. Clearly then, identified ARX models with less parameters are considered *false-negative* results. If false-negatives are found in more than η_{fn} realizations, the value of c should be decreased.

R.4) The dynamics of the selected ARX model $\hat{Y}_p^{\mathrm{best}}$ should be similar to the hypothesized model Y_p^{hyp}. Here, similarity is considered sufficient if the frequency response of $\hat{Y}_p^{\mathrm{best}}$ falls within a predefined range of the magnitude and phase response of Y_p^{hyp}, defined by the inequalities:

$$\frac{1}{\eta_{mag}}|Y_p^{\mathrm{hyp}}(\omega)| < |\hat{Y}_p^{\mathrm{best}}(\omega)| < \eta_{mag}|Y_p^{\mathrm{hyp}}(\omega)|, \tag{7}$$

$$|\angle\hat{Y}_p^{\mathrm{best}}(\omega) - \angle Y_p^{\mathrm{hyp}}(\omega)| < \eta_{phase} \tag{8}$$

The frequency range of interest over which the inequalities are tested, as well as η_{mag} and η_{phase}, are chosen by the user.

All four requirements involve one or more objective thresholds chosen by the user, which will depend on the application. Applications relying on precise predictions of future control inputs, e.g., advanced motion cueing [31], will set more stringent requirements than those that rely on an 'average' HC model, e.g., haptic aids for easy-to-control dynamics [32].

The metric used for R.4 enables the user to objectively decide whether or not $\hat{Y}_p^{\mathrm{best}}$ is sufficiently similar to Y_p^{hyp}. It does not reveal *how* the models differ. This is valuable information if not all requirements can be satisfied simultaneously and changes to the control task or experimental paradigm need to be made. We propose therefore, as an additional analysis method that is *not* part of the tuning process, to *fit the parameters* of Y_p^{hyp} onto $\hat{Y}_p^{\mathrm{best}}$, in the frequency domain, through minimizing a normalized quadratic cost function:

$$\hat{p} = \arg\min_p \left\{ \sum_{i=1}^{n_i} \frac{\left|\hat{Y}_{p_t}^{\mathrm{best}}(\omega_i) - Y_{p_t}^{\mathrm{hyp}}(p;\omega_i)\right|^2}{\left|\hat{Y}_{p_t}^{\mathrm{best}}(\omega_i)\right|^2} + \sum_{i=1}^{n_i} \frac{\left|\hat{Y}_{p_e}^{\mathrm{best}}(\omega_i) - Y_{p_e}^{\mathrm{hyp}}(p;\omega_i)\right|^2}{\left|\hat{Y}_{p_e}^{\mathrm{best}}(\omega_i)\right|^2} \right\} \tag{9}$$

Here, p denotes the parameter vector of the parametric model Y_p^{hyp}, ω_i the ith frequency where the two models are compared, and n_i the number of frequency points. The frequencies ω_i should be spaced logarithmically, to ensure that the fitting does not unduly favor higher frequencies. A genetic algorithm [33] is used to find a reasonably accurate initial estimate of the model parameters, refined by a gradient descend method. This process is performed ten times, from which the parameter set with the lowest cost function is considered the final estimate.

V. Example Identification Problem

The procedure's workflow and performance is illustrated by an example, involving four representative control tasks.

TABLE I
HC MODEL STRUCTURE AND PARAMETER VALUES USED IN SIMULATIONS, UNLESS NOTED OTHERWISE

	$Y_{p_t}^{\mathrm{hyp}}(s)$	K_{p_t}	T_I, s	τ_{p_t}, s	$Y_{p_e}^{\mathrm{hyp}}(s)$	K_{p_e}	T_L, s	τ_{p_e}, s	ω_{nms}, rad/s	ζ_{nms}
SI	$K_{p_t}\frac{1}{Y_c^{\mathrm{SI}}(s)}\frac{1}{(T_I s+1)}e^{-\tau_{p_t}s}$	1	0.28	0.2	$K_{p_e}e^{-\tau_{p_e}s}$	2.3	-	0.21	12	0.2
DI	$K_{p_t}\frac{1}{Y_c^{\mathrm{DI}}(s)}\frac{1}{(T_I s+1)^2}e^{-\tau_{p_t}s}$	1	0.35	0.45	$K_{p_e}(T_L s+1)e^{-\tau_{p_e}s}$	0.45	1.25	0.28	9.5	0.27

In this paper, we present the results for phase 1 only, to validate the proposed procedure using models that are exactly known beforehand. The accompanying experimental study is presented in future work. In this section, the considered control tasks are introduced. Section VI discusses the model selection tuning results, and Section VII presents *how* the selected $\hat{Y}_p^{\mathrm{best}}$ differs from Y_p^{hyp}.

A. Control Tasks

The approach starts by defining the control task to be investigated (step 1), selecting the forcing functions f_t and f_d and the system dynamics Y_c.

1) Forcing functions: Two variations of the target signal f_t will be studied: i) a signal composed of predictable ramp segments (R), and ii) a signal composed of predictable parabola segments (P), see Fig. 5. The unpredictable disturbance signal f_d consists of a sum of ten sines, with the lowest frequency at 0.23 rad/s and the highest frequency at 17.33 rad/s. This signal is identical to the one used in [17].

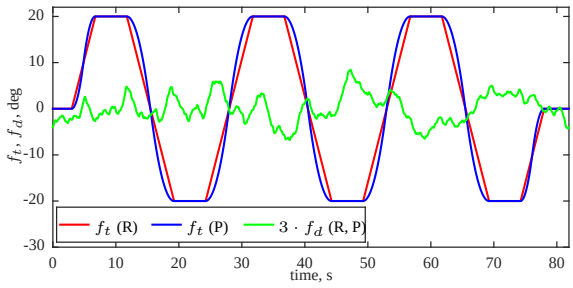

Fig. 5. Two predictable target signals f_t, consisting of ramp and parabola segments, and the quasi-random sum-of-sines disturbance signal f_d.

2) System dynamics: Two common variations of the system dynamics Y_c will be considered: i) a single integrator (SI), Eq. (10), and ii) a double integrator (DI), Eq. (11):

$$Y_c^{\mathrm{SI}}(s) = 1/s \tag{10}$$

$$Y_c^{\mathrm{DI}}(s) = 5/s^2 \tag{11}$$

These represent a wide array of vehicle dynamics [13]. DI dynamics are more difficult to control than SI dynamics, as they require considerable lead action for stability [13].

Each combination of system dynamics and target signal will be referred to with the syntax '{SI,DI}-{R,P}'. E.g., SI-P designates single integrator dynamics and the parabola target.

B. HC Models and Remnant Model

At step 1.2, data is generated through computer simulations with HC models. These simulations require: i) a HC model Y_p^{hyp} that describes the expected HC control behavior, and ii) a noise model to generate the remnant signal n.

1) HC Models: Fig. 6 shows the generic structure of the hypothesized HC model Y_p^{hyp} for all conditions. The HC model structure consists of three components: i) a feedback component $Y_{p_e}^{\mathrm{hyp}}$, ii) a feedforward component $Y_{p_t}^{\mathrm{hyp}}$, and iii) a model of the neuromuscular system Y_{nms}^{hyp} that acts on the summed feedback and feedforward signals: $u_{p_e} + u_{p_t}$. Model details are summarized in Table I.

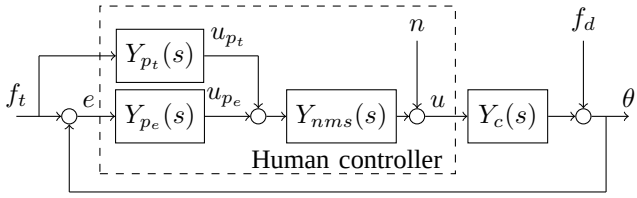

Fig. 6. HC model block diagram.

Literature [17], [18] suggests that the feedback part $Y_{p_e}^{\mathrm{hyp}}$ of the combined feedback-feedforward HC model can be modeled with a structure identical to McRuer's Extended Crossover Model [1]. For an SI, this compensatory model consists of a gain and a time delay; for DI dynamics a lead term parametrized by T_L is added, see the column $Y_{p_e}^{\mathrm{hyp}}(s)$ in Table I. Model parameter values are taken from [17], [18].

The model of the feedforward part $Y_{p_t}^{\mathrm{hyp}}$ is based on the notion that the 'ideal' feedforward controller equals the inverse of the system dynamics [7], [17], [18]. Hence, it consists of a gain, inverse system dynamics $Y_c^{-1}(s)$, an equalization term, and a time delay, see the column $Y_{p_t}(s)$ in Table I.

The equalization term T_I accounts for the possibility that the HC is not able to invert the system dynamics over the entire frequency range, but only up to a certain frequency [18]. Then, τ_{p_t} captures the time delay present in the feedforward response, originating throughout the entire perception and action loop responding to the target signal. The HC might, however, compensate for this delay by anticipating the future course of the target signal, effectively reducing it to zero. The 'perfect' feedforward gain K_{p_t} is 1, but the HC might not be able, or willing, to perform a feedforward action with such strength, as previous studies have shown [17], [18]. Note that for K_{p_t} = 0, the HC model becomes a pure feedback model.

The neuromuscular system (NMS) is modeled with second-

TABLE II
RANGE OF TESTED ARX MODEL ORDERS

	A, B_e, B_{f_t} order			time delay	
	n_a	n_{b_e}	$n_{b_{f_t}}$	n_{k_e}	$n_{k_{f_t}}$
lower bound	1	0	0	1	1
upper bound	7	7	7	15	15

order dynamics [34]:

$$Y_{nms}^{\text{hyp}}(s) = \frac{\omega_{nms}^2}{s^2 + 2\zeta_{nms}\omega_{nms}s + \omega_{nms}^2} \tag{12}$$

Appropriate values for ω_{nms} and ζ_{rms} depend on the system dynamics and were chosen based on [18], see Table I.

2) Remnant Model: Remnant n is added to the control signal u, Fig. 6. It is white noise passed through a third-order low-pass filter (ω_n=12.7 rad/s) with damping (ζ_n=0.26) [26]:

$$H_n(j\omega) = \frac{K_n\omega_n^3}{\left((j\omega)^2 + 2\zeta_n\omega_n j\omega + \omega_n^2\right)(j\omega + \omega_n)}. \tag{13}$$

Here, K_n is used to scale the remnant power such that its variance equals 15% of the variance of the control signal u, during a disturbance-rejection *only* control task: $\sigma_n^2/\sigma_u^2 = 0.15$: the remnant level obtained when averaging five tracking runs. The reason for this is that during the ramp and parabola target-tracking segments, u is not zero-mean, resulting in a large control signal variance which would make the scaled simulated remnant unrealistically large [17].

C. Identification and Parameter Estimation Boundaries

In our procedure the researcher needs to set: i) the range of ARX model orders to be tested at step 1.3, see Section III, ii) the requirements R.1 through R.4 guiding the tuning process at step 1.6, and iii) the lower and upper bounds on the HC model Y_p^{hyp} parameter values during the parametric fitting to assess how $\hat{Y}_p^{\text{best}}$ differs from Y_p^{hyp}.

Table II lists the lower and upper bounds of ARX model orders, defining the ARX models to be estimated and evaluated in step 1.3, identical for all conditions. The least complex models to be tested have only three parameters, the most complex models have 23 free parameters. For each model, the feedforward and feedback time delays are varied between 1 and 15 samples, corresponding to a delay between 0.04 s and 0.60 s which is a reasonably wide range around the true delay values in the simulated HC models, Table I.

At step 1.6 we will impose the following requirements. R.1) False-positive feedforward identification is allowed in fewer than η_{fp} = 2% of the realizations generated with K_{p_t} = 0. R.2) The VAF ratio should be above 0.9 for *all* remnant realizations. R.3) For SI conditions, a model with at least two parameters in the feedforward path ($n_{b_{f_t}} \geq 2$) is necessary to describe inverse system dynamics. For DI conditions, three parameters are necessary ($n_{b_{f_t}} \geq 3$). Models with fewer parameters are considered false-negatives. False-negatives should occur in less than $\eta_{fn} = 25\%$ of realizations for $K_{p_t} = 1$. R.4) Similarity between $\hat{Y}_p^{\text{best}}$ and Y_p^{hyp} is tested between the lowest frequency in f_d (= 0.23 rad/s) and the upper bound of the frequency range that contains 90% of the power of u_{p_t} and u_{p_e} of Y_p^{hyp} for that condition, see Fig. 6. The bounds on magnitude and phase are $\eta_{mag} = 1.5$ and $\eta_{phase} = 45$ deg.

Table III shows the lower and upper bounds on the parameter values of the HC model Y_p^{hyp}, fitted to the selected ARX model to obtain insight in the differences between $\hat{Y}_p^{\text{best}}$ and Y_p^{hyp}. These bounds are identical for all conditions.

TABLE III
RANGE OF HC MODEL PARAMETER VALUES

	K_{p_t} -	T_I s	τ_{p_t} s	K_{p_e} -	T_L s	τ_{p_e} s	ω_{nms} rad/s	ζ_{nms} -
low. b.	0	0	0	0	0	0	5	0
up. b.	2	10	1	10	6	1	20	2

D. Computer Simulations

For each of the four tasks evaluated the hypothesized HC model will be simulated, with the feedforward gain K_{p_t} ranging between 0.0 and 1.0 in steps of 0.1. For each of these 44 (4 $\times$ 11) HC models, one hundred independent remnant realizations will be used.

VI. RESULTS I: TUNING THE MODEL SELECTION CRITERION

A. False-positive Feedforward Model Selection (R.1)

Fig. 7 shows the percentage of remnant realizations for which an ARX model was selected with either $n_{b_{f_t}}$ = 0, 1, 2, ..., or 7, as a function of the model complexity penalty parameter c. For low values of c, and for all conditions, the number of parameters in the feedforward path is relatively high for a considerable number of ARX models: false-positives. When c increases, these false-positives diminish. For $c \geq 3$, in less than 2% of the 100 available remnant realizations a feedforward model is erroneously selected, such that R.1 is met for all conditions. Note that for c = 1, for which the mBIC criterion equals the original BIC, a feedforward model with up to seven orders in the feedforward path is chosen in over 20% of the cases.

B. Time Domain Quality of Fit (R.2)

Requirement R.2 states that the VAF ratio should be above 0.9 for *all* realizations. Fig. 8(a) shows the mean and minimum VAF ratio for all conditions for $K_{p_t} = 0$, for which Y_p^{hyp} is a pure feedback model. For both SI conditions, the mean VAF ratio is equal to 1 for small c, and remains mostly constant as c is made larger; the first notable decrease in the VAF ratio appears only at $c \approx 40$. This indicates that the very high order false-positive feedforward models, selected for $c < 3$, do not provide a truly better fit than models without the feedforward path. The minimum VAF ratio for SI conditions is also close to 1, indicating little variance between realizations. For both DI conditions, however, the minimum VAF ratio is considerably smaller than 1. For DI-P, requirement R.2 is met for $c < 60$. For DI-R, however, the VAF ratio is below 0.9 for *all* values of c, such that requirement R.2 cannot be met.

Then, Fig. 8(b) shows the VAF ratio for all conditions for $K_{p_t} = 1$, for which Y_p^{hyp} is a combined feedback and

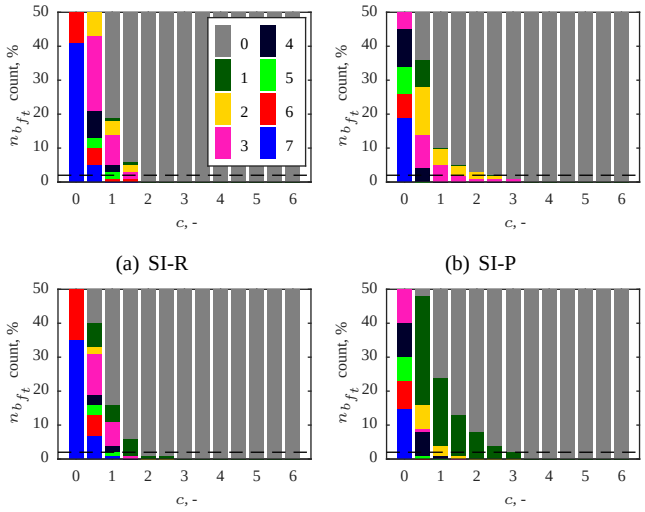

(a) SI-R (b) SI-P

(c) DI-R (d) DI-P

Fig. 7. Percentage of ARX models with $n_{b_{f_t}}$ between 0 and 7, selected from simulated data with $K_{p_t} = 0$, as a function of the model complexity parameter c. All ARX models with $n_{b_{f_t}} > 0$ are false-positives.

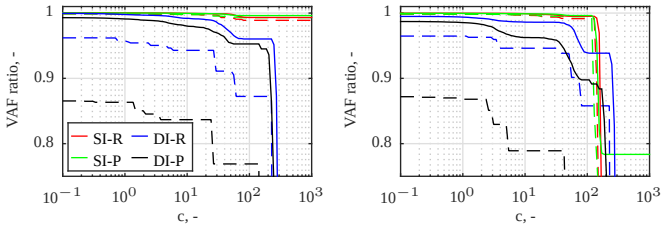

(a) (b)

Fig. 8. Minimum (dashed) and mean (solid) values of VAF($\hat{Y}_p^{\text{best}}$) / VAF(Y_p^{hyp}) taken over all remnant realizations. (a) $K_{p_t} = 0$. (b) $K_{p_t} = 1$.

feedforward model. As for $K_{p_t} = 0$, the mean VAF ratio is larger than 0.9 in SI conditions and DI-P up to large c, such that R.2 can be met. Contrary to $K_{p_t} = 0$, requirement R.2 can also be met for the DI-R condition, but only for $c < 5$.

Note that the VAF ratio tends to decrease in a step-wise fashion; these steps correspond to the 'disappearance' of dynamics in $\hat{Y}_p^{\text{best}}$ that are present in Y_p^{hyp} as c is made larger. The first stepwise decrease for both DI conditions is seen between $c = 1$ and 10, suggesting that 10 is the upper bound for c for avoiding false-negatives. Further analysis will reveal that the disappearing dynamics are the feedforward.

C. Feedforward Model Selection in SI Conditions (R.3)

We then analyze the complexity of models estimated from data generated with HC models that include feedforward, with K_{p_t} between 0.1 and 1.0, to assess 'false-negative' results.

Figs. 9(a) and 9(f) show that for $c = 3$, very few feedforward ARX models are selected for $K_{p_t} = 0.1$ in both SI conditions. That is, for $K_{p_t} = 0.1$ a false-negative result is found in approximately 90% of the simulations. The percentage of selected feedforward ARX models with $n_{b_{f_t}} \geq 2$ much increases for $K_{p_t} \geq 0.2$ in both conditions, reducing the number of false-negative results to approximately 5% for SI-R and 15% for SI-P. For $K_{p_t} \geq 0.3$ no false-negative results are found. For $K_{p_t} = 1$, *all* the selected models contain at least two parameters in the feedforward path, required to describe the inverse system dynamics, and thus R.3 is met.

D. Feedforward Model Selection in DI Conditions (R.3)

Figs. 9(b) and 9(g) show that, for $c = 3$, the number of realizations for which a feedforward model is selected is much smaller in the DI conditions than in the SI conditions. Even for large K_{p_t}, the majority of the selected feedforward models has just one or two parameters in the B_{f_t} polynomial, not sufficient to describe the double differentiator feedforward dynamics, and thus R.3 is *not* met. Hence, the feedforward contribution in both DI conditions, for $c = 3$ and HC model parameter values as given in Table I, is likely to be overseen.

Feedforward ARX models are selected more frequently in the DI-P condition than in the DI-R condition, caused by the relatively larger contribution of the feedforward path to the total control signal. Fig. 10 shows that, for the DI-R condition, u_{p_t} is a sharp pulse of short duration following the onset and endings of the ramp segments. Following this initial transient u_{p_t} is zero, irrespective of the duration or rate of the ramp segment, making identification of the feedforward dynamics difficult. For the DI-P condition, u_{p_t} is a constant, non-zero control input resembling a 'doublet' and persists during the entire parabola segment; here identification of the feedforward dynamics is more straightforward.

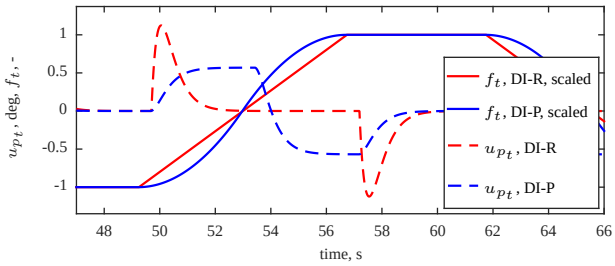

Fig. 10. Feedforward control signal u_{p_t}, in the DI-R and DI-P conditions.

1) Feedforward Model Selection for $c < 3$: If it is deemed acceptable to have false-positive results in more than just 2% of simulations, as required by R.1, c can be made smaller in an effort to identify the small, but perhaps relevant, feedforward contribution in the DI conditions and meet R.3.

Figs. 9(c) and 9(h) show that, for $c = 2$, a considerably larger number of feedforward models are selected. The majority of selected models, however, still contain only one or two parameters in the feedforward path for the DI-R condition. For DI-P, however, choosing $c = 2$ *did* result in a large increase of selected models with $n_{b_{f_t}} \geq 3$, especially for $K_{p_t} \geq 0.5$.

Finally, Figs. 9(d) and 9(i) illustrate how the distribution of selected models changes when c is reduced further to 1, for which the mBIC is equal to the original BIC. For $K_{p_t} = 0$ many false-positive results are found and for $K_{p_t} \geq 0.1$ many models are selected with just one parameter in the B_{f_t} polynomial, that clearly do not model Y_p^{hyp} correctly. This demonstrates the importance of choosing a value of c that is large enough to prevent false-positive results.

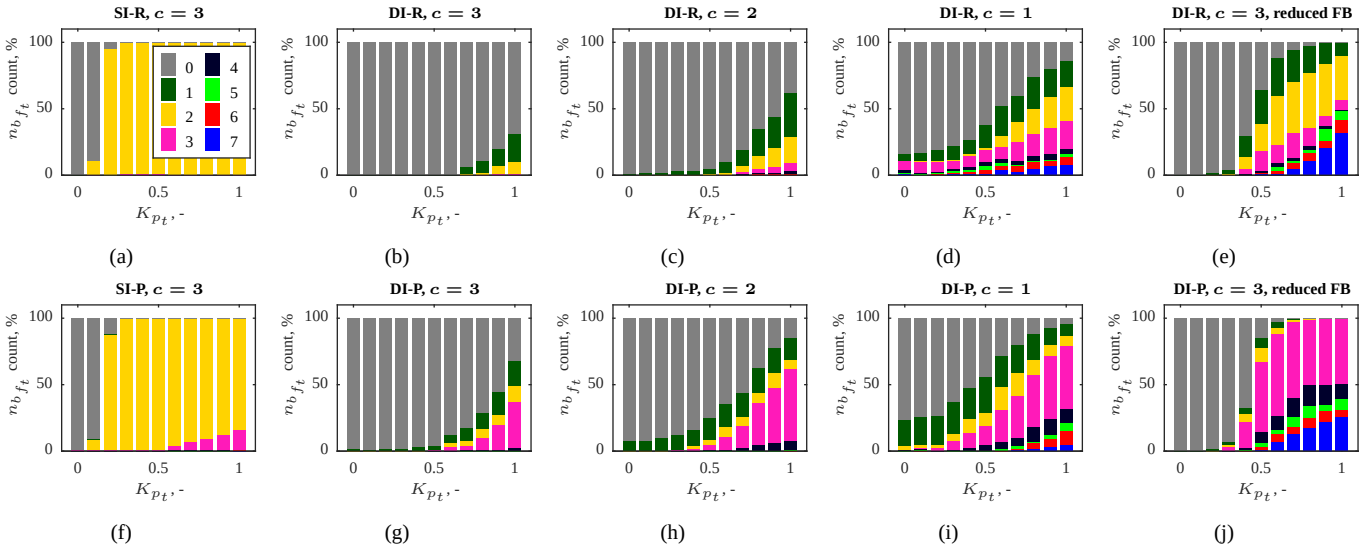

Fig. 9. Percentage cases for which an ARX model with an indicated number of parameters in the feedforward path was identified, as a function of K_{p_t}.

2) Effects of Feedback Gain on Feedforward Model Selection: To illustrate the effect of the relative strength of the feedforward and feedback paths on the detection of the correct model, further simulations with reduced feedback gains were performed for the DI conditions. The feedback gain K_{p_e} was reduced by 30% to 0.32 and the lead time constant T_L set at 1 s. The effects are considerable: compare Figs. 9(b) and 9(g) to Figs. 9(e) and 9(j), respectively. The number of (correctly) selected feedforward ARX models with $n_{b_{f_t}} \geq 3$ is much larger for $K_{p_t} > 0.5$, especially in the DI-P condition.

E. Similarity between $\hat{Y}_p^{\text{best}}$ and Y_p^{hyp} (R.4)

Fig. 11 shows a Bode plot of $\hat{Y}_p^{\text{best}}$, for 40 different remnant realizations of the SI-P condition ($K_{p_t} = 0.3$; $c = 3$) compared to the true model Y_p^{hyp}. Green dashed lines indicate the boundaries corresponding to R.4, for the frequency range over which R.4 is tested. 90% of the power of u_{p_t} is at very low frequencies (< 0.8 rad/s); u_{p_e} has a more uniform power distribution, and thus similarity is tested over a wider range. The majority of the models fall within the boundaries. Thus, we conclude that both the feedforward and feedback paths are sufficiently similar to Y_p^{hyp}.

At higher frequencies, two 'clusters' of similar solutions are seen: models that show the NMS peak, marked 1}, and models that lack this peak, marked 2}. Models belonging to the second cluster have fewer parameters in the A polynomial. Models without NMS dynamics in the feedforward path also lack these dynamics in the feedback path, as they are included in both, Fig. 4. The NMS contribution is small and mostly present at higher frequencies, where remnant dominates. In 25% of the cases the contribution of the NMS was apparently too small and 'drowned' in the remnant noise to overcome the penalty of added complexity, and is not present in the model. For larger values of K_{p_t} the selected ARX models resemble Y_p^{hyp} much better for $\omega < 3$ rad/s (not shown). That is, the results shown for $K_{p_t} = 0.3$ illustrate 'worst case' results.

Fig. 12 shows a Bode plot of $\hat{Y}_p^{\text{best}}$, for 40 different remnant realizations of the DI-P condition, for $K_{p_t} = 1$, compared to Y_p^{hyp}, if c is reduced to 2, see Section VI-D1. Again, results appear in 'clusters'. Here, these clusters correspond to the number of parameters in the B_{f_t} polynomial, as annotated in the figure caption. The models with $n_{b_{f_t}} \geq 3$ are similar to Y_p^{hyp}, in the sense that they are a double differentiator for $\omega < 2$ rad/s, but only few fall within the bounds of R.4. For $c = 3$, even fewer models fall within the bounds.

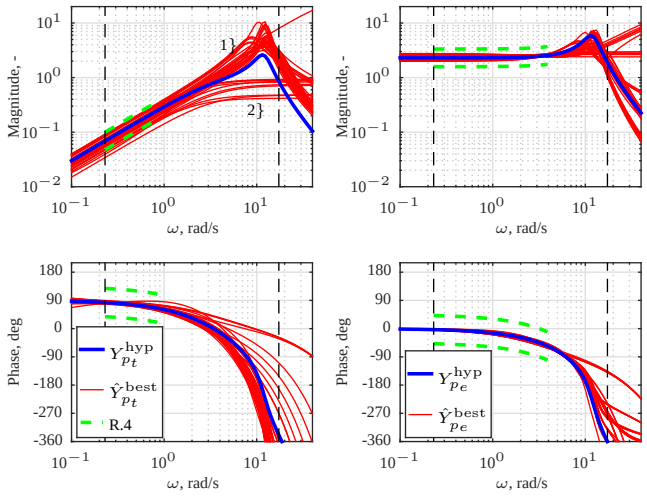

Fig. 11. Bode plots of $\hat{Y}_p^{\text{best}}$, SI-P ($c = 3$, $K_{p_t} = 0.3$), other parameter values as given in Table I. Dashed lines indicate boundaries imposed by R.4, drawn for the frequency range over which R.4 is tested.

Fig. 13 shows the percentage of remnant realizations for which $\hat{Y}_p^{\text{best}}$ was sufficiently similar to Y_p^{hyp}, for $c = 3$, as tested by (7) and (8), for all conditions and all values of K_{p_t}. For both SI conditions, $\hat{Y}_p^{\text{best}}$ is sufficiently similar to Y_p^{hyp} for all realizations for $K_{p_t} \geq 0.5$. In the DI-P condition, the similarity is sufficient in a few cases for $K_{p_t} \geq 0.7$. For the simulations performed with lower feedback gains, see Section VI-D2, the similarity is sufficient in more cases, but

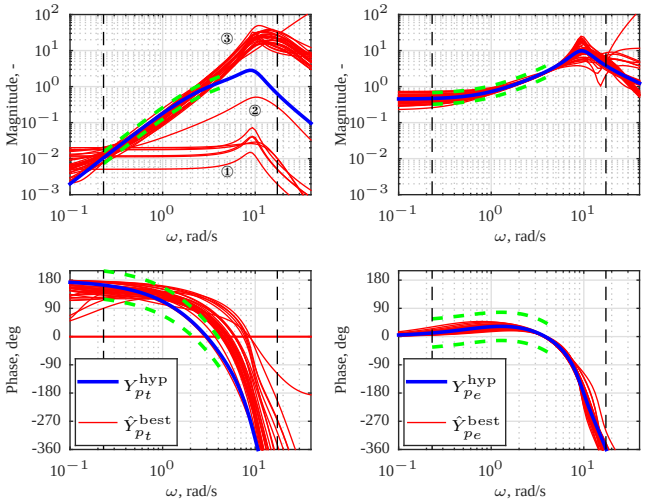

(a) feedforward (b) feedback

Fig. 12. Bode plots of $\hat{Y}_p^{\text{best}}$ compared to Y_p^{hyp}, condition DI-P, $c = 2$, $K_{p_t} = 1$, other parameter values as given in Table I. Clusters of results: 1} correspond to $n_{b_{f_t}} = 1$; 2} $n_{b_{f_t}} = 2$; 3} $n_{b_{f_t}} \geq 3$. Dashed lines indicate boundaries imposed by R.4, drawn for the frequency range over which R.4 is tested.

still not 100%. For DI-R, $\hat{Y}_p^{\text{best}}$ is never sufficiently similar; neither for the parameter set of Table I nor for the lower feedback gains. This confirms the results obtained for R.3.

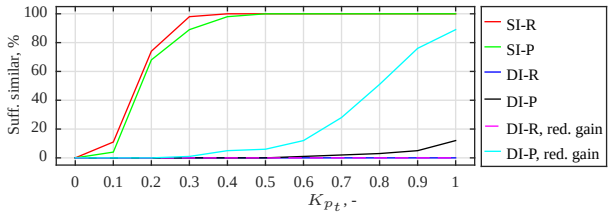

Fig. 13. The percentage of remnant realizations for which $\hat{Y}_p^{\text{best}}$ is sufficiently similar to Y_p^{hyp}, for $c = 3$.

F. Conclusions

Based on the presented results we conclude that, first, the identification procedure can identify small feedforward contributions ($K_{p_t} \geq 0.3$) for all SI conditions, when choosing $c = 3$, which provides a probability less than 2% of obtaining a false-positive result. Second, the procedure can identify the feedforward contribution in the DI-P condition only if the feedforward contribution is relatively large when choosing $c = 3$. Third, the procedure *cannot* properly identify the feedforward contribution in the DI-R condition without greatly reducing the value of c, which increases the risk of obtaining false-positive results. Hence, the procedure is suitable to analyze experimental human-in-the-loop data of both SI conditions and the DI-P condition.

VII. Results II: Analysis of $\hat{Y}_p^{\text{best}}$- Y_p^{hyp} Similarity

Requirement R.4 allows the user to test the similarity between $\hat{Y}_p^{\text{best}}$ and Y_p^{hyp} in an objective, quantitative way, but does not reveal *how* $\hat{Y}_p^{\text{best}}$ differs from Y_p^{hyp}. To obtain insight, the parametric model Y_p^{hyp} is fit onto $\hat{Y}_p^{\text{best}}$, and the parameter estimates are compared to the true values.

1) SI Conditions: Figs. 14(a)-(g) show the HC model parameter estimates, for each individual remnant realization, for both SI conditions. Note that the results are shown only for the $\hat{Y}_p^{\text{best}}$ models for which $n_{b_{f_t}} \geq 2$. All individual results are plotted in a scatter-plot, to explicitly show their distributions.

The feedforward gain K_{p_t}, varied between 0.0 and 1 (steps of 0.1) in the simulations, is estimated close to the real value with little variance, Fig. 14(a). Bias and variance is smaller in the SI-R condition than in the SI-P condition, suggesting that the ramp target signal is more suited for the correct detection of feedforward. Note that for $0.1 \leq K_{p_t} \leq 0.2$ (for which false-negative results were found in some cases) the bias and variance is of the same magnitude as for $K_{p_t} \geq 0.3$, for which no false-negative results were found. Hence, *if* a feedforward model is selected, the model has the correct feedforward gain.

Fig. 14(b) shows the estimate of the feedforward equalization parameter T_I. Whereas in the SI-R conditions T_I is estimated close to zero for $K_{p_t} < 0.6$, and close to the true value for $K_{p_t} \geq 0.6$, for the SI-P conditions the estimate is bad. The effects of T_I are larger during the onsets of ramp segments, as compared to the onsets of parabolas. Hence, a reliable estimate of T_I is possible only in the SI-R conditions from models with a strong feedforward component. If it is deemed important that T_I is estimated with higher accuracy, a target signal needs to be designed with a higher power at frequencies where T_I has an effect. Changes made to f_t would, however, likely also cause the control behavior to change [35].

The feedforward time delay τ_{p_t} is estimated equal to integer multiples of the 0.04 s sample time, Fig. 14(c). For all SI conditions τ_{p_t} is overestimated, with a large variance and slightly smaller bias when K_{p_t} increases. The bias in the estimates for τ_{p_t} is likely caused by the interaction between T_I and τ_{p_t}, as both parameters cause lag in Y_{p_t}. That is, most of the dynamics caused by the T_I parameter can be described by choosing a slightly larger value for $n_{k_{f_t}}$, *without any added cost* to the model complexity, such that these models are likely to be preferred by the selection criterion.

Fig. 14(d) shows that the feedback gain K_{p_e} is estimated with moderate bias and variance. Furthermore, the quality of the estimate is mostly unaffected by the variation in K_{p_t}. If a higher similarity between $\hat{Y}_p^{\text{best}}$ and Y_p^{hyp} with respect to the feedback gain is desired, remnant levels need to be reduced, e.g., by averaging the data over more than five runs [26].

Fig. 14(e) shows a multimodal distribution in the estimates of the feedback time delay τ_{p_e}, with a density peak around 0.20 s (close to the real value of 0.21 s), and smaller peaks around 0.08, 0.12, and 0.16 s. This is caused by the delay parameter n_{k_e} that is equal to an integer multiple of the sample time of 0.04 s. The bias towards lower values is likely a result of the interaction between τ_{p_e} and the NMS parameters, Figs. 14(f) and 14(g). As shown by Fig. 11(b), 90% of the signal power of u_{p_e} is located below 5 rad/s, resulting in a bad estimation of dynamics affecting higher frequencies. Especially the ζ_{nms} estimates have a large bias and variance, indicating that the identification procedure is unable to successfully capture the NMS effects in these

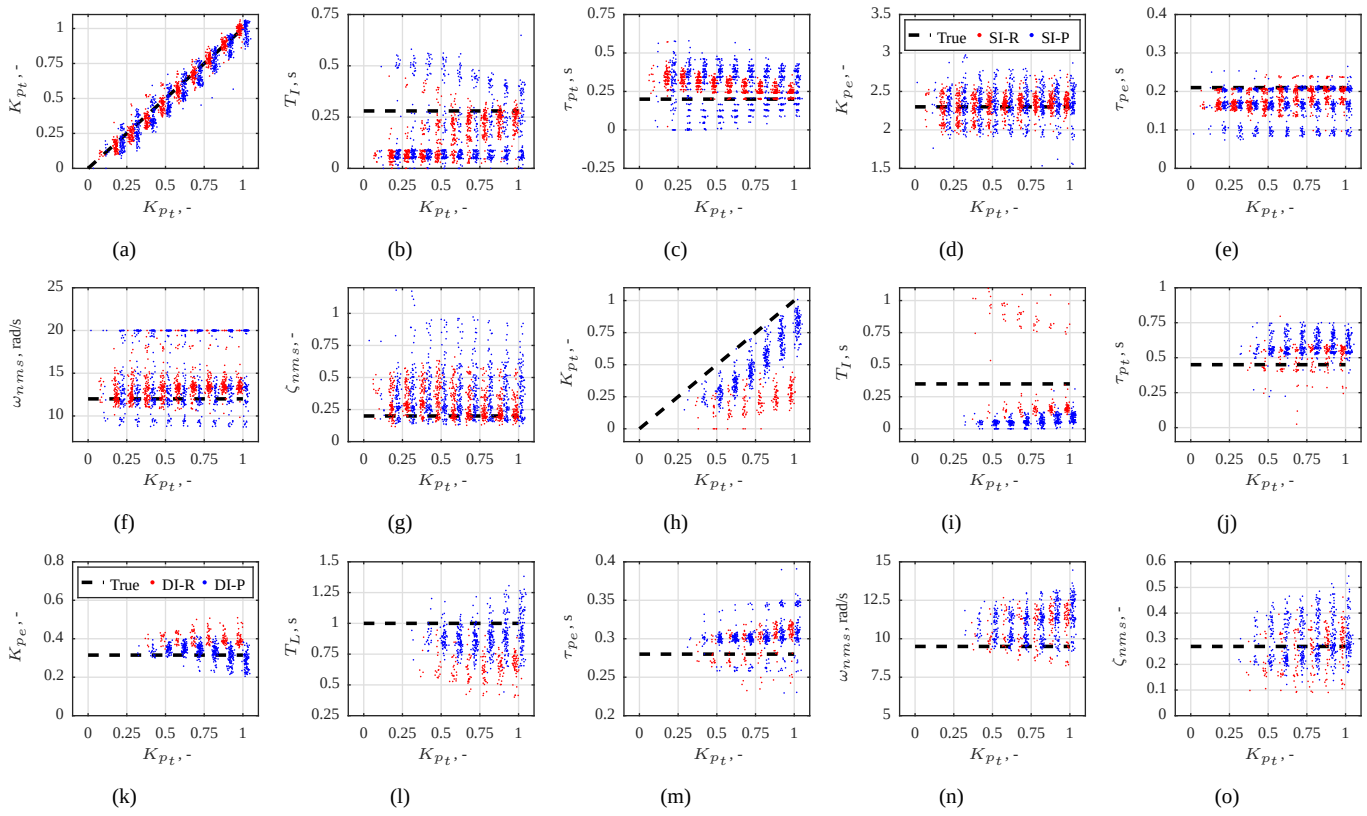

Fig. 14. The identified values of each HC model parameter for each individual remnant realization compared to the real value. (a) through (g) show results for the SI-R and SI-P conditions, with HC model parameter values as given in Table I, and $c = 3$. (a) K_{p_t}, (b) T_I, (c) τ_{p_t}, (d) K_{p_e}, (e) τ_{p_e}, (f) ω_{nms}, (g) ζ_{nms}. (h) through (o) show results for the DI-R and DI-P conditions, with $K_{p_e} = 0.32$, $T_L = 1$ s, and all other HC model parameter values as given in Table I, and $c = 3$. (h) K_{p_t}, (i) T_I, (j) τ_{p_t}, (k) K_{p_e}, (l) T_L, (m) τ_{p_e}, (n) ω_{nms}, (o) ζ_{nms}.

conditions, see also Fig. 11. If it is deemed important that the NMS dynamics are estimated with higher accuracy, the power distribution in f_d needs to be changed. This might also affect the HC control behavior [35].

To conclude, in the SI conditions the model selection criterion selects a model that describes the underlying dynamics 'efficiently'. It is not more complex than strictly necessary and in many cases a slightly worse quality of fit is accepted in return for a reduction in model complexity.

2) DI Conditions: Only a few feedforward ARX models with $n_{b_{f_t}} > 2$ were selected from simulations with the parameter values of Table I, but many from simulations with a reduced feedback contribution in the DI-P condition, as discussed in Section VI-D2. Hence, for the initial simulations it was possible only to estimate the feedback parameters. As these estimates were very similar to those for the simulations with reduced feedback gains, we only show the latter in Figs. 14(h) through 14(o). Results only include selected models with $n_{b_{f_t}} \geq 3$, hence far more results are shown for the DI-P than DI-R conditions (see also Figs. 9(e) and 9(j)). The few remaining parameter estimates for the DI-R condition show large biases, confirming that the procedure cannot identify HC dynamics in the DI-R condition.

The feedforward parameter estimates for the DI-P condition, Figs. 14(h) through 14(j), show notable biases with considerable variance, but do illustrate that $\hat{Y}_{p_t}^{\text{best}}$ is a reasonably accurate representation of $Y_{p_t}^{\text{hyp}}$. K_{p_t} is generally underestimated with a large variance, whereas the delay τ_{p_t} is overestimated by approximately 200 ms. Bode plots (Fig. 12(a)) revealed that all selected $\hat{Y}_p^{\text{best}}$ models indeed lack the effect of T_I, i.e., they are a double differentiator up to $\omega = 10$ rad/s, whereas Y_p^{hyp} becomes a single differentiator around $\omega = 1/T_I = 2.8$ rad/s. The effect of T_I is apparently too small to be captured and as a consequence its value is estimated close to zero.

Considerable variances in estimates are found for all feedback parameters, but with small biases, see Figs. 14(k) - 14(m). NMS parameter estimates show considerable biases and variances, Figs. 14(n) - Fig. 14(o).

A variety of changes can be made to the DI-P condition if more accurate feedforward identification is desired. The power of f_t relative to f_d can be increased to emphasize feedforward, at the expense of accuracy of feedback identification. Furthermore, reducing the remnant level by averaging over more tracking runs is expected to improve identification results, but note that HC control behavior might not be constant throughout many repetitive runs.

VIII. Discussion

Given a particular manual control task, it is often not known a priori whether the HC will exert feedforward control, or how the HC feedforward and feedback paths should be modeled. Prior assumptions on the feedforward or feedback dynamics cannot be made based on previous experimental results, because hardly any literature exists on the subject.

This paper presents a new LTI-model based identification procedure, to more objectively identify the feedforward and feedback components of HC control behavior without making any prior assumptions on the HC dynamics. The novel feature of this procedure is the *objective* selection of the correct model, based on a model selection criterion that is tuned by means of simulations *prior* to collecting experimental data.

The introduced procedure is successful in answering if and how the HC responds to f_t and e for three of the four control task conditions studied in this paper. For the SI-R, SI-P, and DI-P conditions, the procedure correctly identified the characteristic features of the feedforward and feedback controller dynamics from a noisy data set, making the procedure suitable for O.1 and O.2. False-positive detection of a feedforward response from data generated by a purely feedback model is prevented by tuning the model selection criterion. False-negative results, i.e., the selection of a purely feedback model from data generated by a combined feedback-feedforward model, occur only for data generated with small feedforward gains ($K_{p_t} \leq 0.3$) in both SI conditions. For the DI-P condition, false-negative results occur for a larger range of K_{p_t} values, and depend much on the relative strength of the feedforward and feedback paths.

The procedure is able to correctly identify the governing low-frequency dynamics of the HC responses. More subtle dynamics, such as feedforward equalization and time delays, are estimated, if at all, with large biases. Hence, the results of this procedure alone are not sufficient to build a parametrized HC model (O.3). A gray-box modeling approach is required to obtain the HC model with the correct parametrization.

In the DI-R conditions, the contribution of the feedforward path is small and is identified only sporadically from the noisy data. To improve the identification accuracy in this condition, one could evaluate the ARX models *only* on the segments where feedforward is expected, such as the ramp onsets and endings. This method was reported in [18], who used a time-domain parameter estimation method. Evaluating this approach for ARX models is beyond the current scope.

Our identification procedure includes three features to ensure objective model selection, which were not previously applied in the identification of manual control behavior. These features are: i) the use of a separate estimation and validation data set to prevent overfitting, ii) the use of a model selection criterion that makes an explicit trade-off between model quality and model complexity, and iii) the tuning of this explicit trade-off by means of simulated data.

Our results demonstrate that the use of the standard BIC results in many false-positive results, and thus the selection criterion needs to be modified by choosing an appropriate value for the c parameter. Other model selection criteria exist, such as the Akaike Information Criterion (AIC) [36], but these criteria generally penalize model complexity even less than the BIC and would not be suitable in the current application.

We argue that performing Monte Carlo simulations using a hypothesized model is the most objective way to gain insight in the identification process and tune c appropriately. It evaluates the identification process for a case similar to the real case, and for which the ground truth is known, leaving the least room for any subjective interpretation. The Monte Carlo simulations simultaneously assess the ability of the identification procedure to estimate the correct model from measurements made in closed-loop, and deal with the high levels of human remnant (colored white noise).

The main disadvantage of the features included to prevent false-positive results are possible false-negative results, i.e., existing controller dynamics that are not identified, or dynamics that are identified with a relatively large bias. For instance, the effects of the feedforward bandwidth parameter T_I are missing from the selected models in the DI-P condition: this is essentially a false-negative result. Accurate tuning of the model selection criterion should prevent most false-positive occurrences, but for certain conditions a compromise will have to be found between false-positive and false-negative results.

The presented identification procedure is part of a complete approach to studying manual control behavior, which involves simulations and experimental data and has an iterative nature. This paper presented the simulation results, from which we conclude that, apart from the DI-R condition, an experimental study can be performed to answer if and how the HC responds to the target signals and system dynamics evaluated. Clearly, if the experimentally obtained HC dynamics are very different from the hypothesized HC dynamics, the whole tuning procedure should be repeated with an HC model closer to the HC behavior found experimentally.

The tuning process is guided by four objective requirements, determined by the user based on the application. These four requirements can additionally be used to compare the performance of this procedure with novel methods in the future.

The proposed procedure is considered to be particularly useful in studies that involve multi-loop or multi-modal HC behavior, which generally require more complex HC models to describe the measured behavior. For the first time, we showed that in dealing with these more complex models false-positives occur more frequently than one would expect, which casts serious doubts upon the validity of many previous findings.

IX. Conclusions

We introduced an objective procedure to identify if and how the human controller utilizes feedforward and feedback, in control tasks with predictable target signals and unpredictable disturbances. The procedure aims to identify HC dynamics in closed loop, from noisy data, and without making any prior assumptions regarding the HC model structure or parameters. It estimates and evaluates a large number of LTI ARX model candidates and uses a novel model selection criterion to select the best model. The original Bayesian Information Criterion was found to return many false-positive results: models that contain dynamics not present in the measured system. We demonstrate that in identifying HC dynamics, it is mandatory to increase the penalty imposed on the model order, through a model complexity penalty parameter. The appropriate value of this parameter can be found through Monte Carlo computer simulations with a hypothesized HC model, guided by four objective requirements chosen by the user. To illustrate its performance, the procedure was applied to four typical manual

control tasks, with single and double integrator dynamics, and predictable target signals composed of ramp and parabola segments. The procedure was able to identify the correct HC model structure for both target signals with the single integrator dynamics, and for the parabola target signal with the double integrator. The identification for HC behavior with double integrator dynamics and ramp targets proved to be problematic, confirming previous results.

REFERENCES

[1] D. T. McRuer, D. Graham, E. S. Krendel, and W. J. Reisener, "Human Pilot Dynamics in Compensatory Systems, Theory Models and Experiments with Controlled Element and Forcing Function Variations," Air Force Flight Dynamics Laboratory, Tech. Rep. AFFDL-TR-65-15, 1965.

[2] E. R. Boer and R. V. Kenyon, "Estimation of Time-Varying Delay Time in Nonstationary Linear Systems: An Approach to Monitor Human Operator Adaptation in Manual Tracking Tasks," *IEEE Trans. on Systems, Man & Cybernetics – Part A: Systems and Humans*, vol. 28, no. 1, pp. 89–99, 1998.

[3] R. A. Hess, J. K. Moore, and M. Hubbard, "Modeling the Manually Controlled Bicycle," *IEEE Trans. on Systems, Man & Cybernetics, Part A: Systems and Humans*, vol. 42, no. 3, pp. 545–557, 2012.

[4] J. J. Potter and W. Singhose, "Improving Manual Tracking of Systems with Oscillatory Dynamics," *IEEE Trans. on Human-Machine Systems*, vol. 43, no. 1, pp. 46–52, 2013.

[5] K. Van der El, D. M. Pool, H. J. Damveld, M. M. Van Paassen, and M. Mulder, "An Empirical Human Controller Model for Preview Tracking Tasks," *IEEE Transactions on Cybernetics*, Accepted for publication.

[6] E. S. Krendel and D. T. McRuer, "A Servomechanics Approach to Skill Development," *J. of the Franklin Inst.*, vol. 269, no. 1, pp. 24–42, 1960.

[7] R. J. Wasicko, D. T. McRuer, and R. E. Magdaleno, "Human Pilot Dynamic Response in Single-loop Systems with Compensatory and Pursuit Displays," Air Force Flight Dynamics Laboratory, Tech. Rep. AFFDL-TR-66-137, 1966.

[8] R. E. Magdaleno, H. R. Jex, and W. A. Johnson, "Tracking Quasi-Predictable Displays Subjective Predictability Gradations, Pilot Models for Periodic and Narrowband Inputs," in *Fifth Annual Conf. on Manual Control, Cambridge (MA), March 27-29*, 1969, pp. 391–428.

[9] A. J. Bastian, "Learning to Predict the Future: the Cerebellum Adapts Feedforward Movement Control," *Current Opinion in Neurobiology*, vol. 16, pp. 645–649, 2006.

[10] A. J. Nagengast, D. A. Braun, and D. M. Wolpert, "Optimal Control Predicts Human Performance on Objects with Internal Degrees of Freedom," *PLOS Computational Biology*, vol. 5, p. e1000419, 2009.

[11] S. Franklin, D. M. Wolpert, and D. W. Franklin, "Visuomotor Feedback Gains Upregulate during the Learning of Novel Dynamics," *J. of Neurophysiology*, vol. 108, pp. 467–478, 2012.

[12] B. Nasseroleslami, C. J. Hasson, and D. Sternad, "Rhythmic manipulation of objects with complex dynamics: Predictability over chaos," *PLoS Comput Biol*, vol. 10, no. 10, p. e1003900, 10 2014.

[13] D. T. McRuer and H. R. Jex, "A Review of Quasi-Linear Pilot Models," *IEEE Trans. on Human Factors in Electronics*, vol. 8, no. 3, pp. 231–249, 1967.

[14] R. A. Hess, "Pursuit Tracking and Higher Levels of Skill Development in the Human Pilot," *IEEE Trans. on Systems, Man & Cybernetics*, vol. 11, no. 4, pp. 262–273, 1981.

[15] R. W. Pew, J. C. Duffendack, and L. K. Fensch, "Sine-Wave Tracking Revisited," *IEEE Trans. on Human Factors in Electronics*, vol. 8, no. 2, pp. 130–134, 1967.

[16] T. Yamashita, "Effects of Sine Wave Combinations on the Development of Precognitive Mode in Pursuit Tracking," *The Quarterly J. of Experimental Psychology*, vol. 42A, no. 4, pp. 791–810, 1990.

[17] F. M. Drop, D. M. Pool, H. J. Damveld, M. M. van Paassen, and M. Mulder, "Identification of the Feedforward Component in Manual Control With Predictable Target Signals," *IEEE Trans. on Cybernetics*, vol. 43, no. 6, pp. 1936–1949, 2013.

[18] V. A. Laurense, D. M. Pool, H. J. Damveld, M. M. van Paassen, and M. Mulder, "Effects of Controlled Element Dynamics on Human Feedforward Behavior in Ramp-Tracking Tasks," *IEEE Trans. on Cybernetics*, vol. 45, no. 2, pp. 253–265, 2015.

[19] B. Yu, J. S. Freudenberg, and R. B. Gillespie, "Human Control Strategies in Pursuit Tracking with a Disturbance Input," in *Proc. of the 53rd IEEE Conf. on Decision and Control, Los Angeles (CA), Dec. 15-17*, 2014.

[20] A. van Lunteren, "Identification of Human Operator Describing Function Models with One or Two Inputs in Closed Loop Systems," Ph.D. dissertation, TU Delft, Fac. of Mechanical Engineering, 1979.

[21] S. M. Shinners, "Modeling of human operator performance utilizing time series analysis," *IEEE Trans. on Systems, Man & Cybernetics*, vol. 4, no. 5, pp. 446–458, 1974.

[22] F. Osafo-Charles, G. Agarwal, W. D. O'Neill, and G. L. Gottlieb, "Application of time-series modeling to human operator dynamics," *IEEE Trans. on Systems, Man & Cybernetics*, vol. 10, no. 12, pp. 849–860, 1980.

[23] A. Abdel-Malek and V. Z. Marmarelis, "Modeling of Task-Dependent Characteristics of Human Operator Dynamics Pursuit Manual Tracking," *IEEE Trans. on Systems, Man & Cybernetics*, vol. 18, no. 1, pp. 163–172, 1988.

[24] M. M. van Paassen and M. Mulder, "Identification of Human Operator Control Behaviour in Multiple-Loop Tracking Tasks," in *Proc. of the Seventh IFAC/IFIP/IFORS/IEA Symp. on Analysis, Design and Evaluation of Man-Machine Systems, Kyoto, Japan*, 1998, pp. 515–520.

[25] F. M. Nieuwenhuizen, P. M. T. Zaal, M. Mulder, M. M. van Paassen, and J. A. Mulder, "Modeling Human Multichannel Perception and Control Using Linear Time-Invariant Models," *J. of Guidance, Control, and Dynamics*, vol. 31, no. 4, pp. 999–1013, 2008.

[26] P. M. T. Zaal, D. M. Pool, Q. P. Chu, M. M. van Paassen, M. Mulder, and J. A. Mulder, "Modeling Human Multimodal Perception and Control Using Genetic Maximum Likelihood Estimation," *J. of Guidance, Control, and Dynamics*, vol. 32, no. 4, pp. 1089–1099, 2009.

[27] L. Ljung, *System Identification Theory for the User*, 2nd ed. Prentice Hall, Inc., 1999.

[28] G. Schwarz, "Estimating the dimension of a model," *Annals of Statistics*, vol. 6, no. 2, pp. 461–464, 1978.

[29] D. T. McRuer and E. S. Krendel, "Mathematical Models of Human Pilot Behavior," Advisory Group for Aerospace Research and Development, AGARDograph AGARD-AG-188, 1974.

[30] P. M. J. van den Hof, "Closed-loop issues in system identification," *Annual Reviews in Control*, vol. 22, pp. 173 – 186, 1998.

[31] A. Beghi, M. Bruschetta, and F. Maran, "A real-time implementation of an mpc-based motion cueing strategy with time-varying prediction," in *Systems, Man, and Cybernetics (SMC), 2013 IEEE International Conference on*, Oct 2013, pp. 4149–4154.

[32] M. Olivari, F. M. Nieuwenhuizen, H. H. Bülthoff, and L. Pollini, "Pilot adaptation to different classes of haptic aids in tracking tasks," *AIAA Journal of Guidance, Control, and Dynamics*, vol. 37, no. 6, pp. 1741–1753, Dec. 2014.

[33] D. E. Goldberg and J. H. Holland, "Genetic algorithms and machine learning," *Machine Learning*, vol. 3, no. 2-3, pp. 95–99, 1988.

[34] D. T. McRuer, R. E. Magdaleno, and G. P. Moore, "A Neuromuscular Actuation System Model," *IEEE Trans. on Man-Machine Systems*, vol. 9, no. 3, pp. 61–71, 1968.

[35] G. C. Beerens, H. J. Damveld, M. Mulder, M. M. van Paassen, and J. C. van der Vaart, "Investigation into Crossover Regression in Compensatory Manual Tracking Tasks," *J. of Guidance, Control, and Dynamics*, vol. 32, no. 5, pp. 1429–1445, 2009.

[36] H. Akaike, "A New Look at the Statistical Model Identification," *IEEE Trans. on Automatic Control*, vol. 19, no. 6, pp. 716–723, 1974.